Applied Catalysis B: Environmental 150–151 (2014) 479–485

Contents lists available at ScienceDirect

Applied Catalysis B: Environmental

journal homepage: www.elsevier.com/locate/apcatb

Complete oxidation of acetaldehyde over a composite photocatalyst of graphitic carbon nitride and tungsten(VI) oxide under visible-light irradiation

Zhengyuan Jin[a], Naoya Murakami[a], Toshiki Tsubota[a], Teruhisa Ohno[a,b,c,*]

[a] Department of Applied Chemistry, Faculty of Engineering, Kyushu Institute of Technology, 1-1 Sensuicho, Tobata, Kitakyushu 804-8550, Japan
[b] JST, PRESTO, 4-1-8 Honcho Kawaguchi, Saitama 332-0012, Japan
[c] JST, ACT-C, 4-1-8 Honcho Kawaguchi, Saitama 332-0012, Japan

ARTICLE INFO

Article history:
Received 4 October 2013
Received in revised form
19 December 2013
Accepted 28 December 2013
Available online 7 January 2014

Keywords:
$g\text{-}C_3N_4$
WO_3
Photocatalysis
Planetary mill
Z-scheme

ABSTRACT

Graphitic carbon nitride ($g\text{-}C_3N_4$) was prepared by heating melamine and then its specific surface area was enlarged by hydrothermal treatment in aqueous sodium hydroxide solution. The $g\text{-}C_3N_4$ samples were blended with tungsten(VI) oxide (WO_3) using a planetary mill in order to improve photocatalytic activity. The composite photocatalyst with optimized amounts of these contents showed higher photocatalytic activity for decomposition of acetaldehyde under visible-light irradiation than did original samples. From the results, we concluded that the composite photocatalyst utilizes both high oxidation ability of WO_3 and high reduction ability of $g\text{-}C_3N_4$ by *Z*-scheme charge transfer.

1. Introduction

Titanium(IV) oxide (TiO_2) is the most widely used photocatalyst because of its excellent oxidation ability, availability and stability [1]. However, there are two major problems with a conventional TiO_2 photocatalyst: it is inactive under visible-light irradiation and it has low quantum efficiency due to a high recombination rate of photogenerated electron-hole pairs. There have been numerous studies on TiO_2 with impurity doping [2,3], co-catalyst loading [4] and shape control [5,6] for improvement of visible-light response and reaction efficiency of electrons and holes, though these methods still have limitations for improvement of solar energy conversion efficiency.

It is rather challenging to design a semiconductor photocatalyst fulfilling the multiple requirements. Actually, a single semiconductor with large visible-light absorption has difficulty in exhibiting both high reduction and oxidation abilities due to its narrow bandgap structure. Therefore, a composite photocatalyst consisting of different kinds of semiconductors has been studied in recent years. Some studies showed that an appropriate composition of two kinds of photocatalyst enhanced photocatalytic activity as a result of charge separation between two semiconductors [7–12]. This mechanism employs interparticle electron transfer to one semiconductor with a more positive conduction band (CB) potential and hole transfer to the other semiconductor with a more negative valence band (VB) potential. Thus, this kind of composite photocatalyst cannot utilize both high reduction and oxidation abilities. In contrast, another reaction mechanism for a composite photocatalyst, namely, *Z*-scheme reaction mechanism, has been suggested in several reports [13–17]. This mechanism enables a composite photocatalyst to utilize both reduction ability for one semiconductor with more negative CB potential and oxidation ability for another semiconductor with more positive VB potential as a result of two-step excitation. Thus, a *Z*-scheme composite photocatalyst is one means for utilizing both high oxidation and reduction abilities under visible-light irradiation if appropriate semiconductors are used.

In our previous study, a composite of graphitic carbon nitride ($g\text{-}C_3N_4$), which is an organic semiconductor with visible-light absorption, high reduction ability and high chemical stability [18], with sulfur-doped TiO_2 was made [19]. In that study, the composite sample prepared by a planetary mill showed high photocatalytic activity for acetaldehyde decomposition under visible-light irradiation as a result of *Z*-scheme charge transfer. Thus, the sample

* Corresponding author at: Department of Applied Chemistry, Faculty of Engineering, Kyushu Institute of Technology, 1-1 Sensuicho, Tobata, Kitakyushu 804-8550, Japan. Tel.: +81 93 884 3318; fax: +81 93 884 3318.
E-mail address: tohno@che.kyutech.ac.jp (T. Ohno).

0926-3373/$ – see front matter © 2014 Elsevier B.V. All rights reserved.
http://dx.doi.org/10.1016/j.apcatb.2013.12.048

showed both high oxidation ability of sulfur-doped TiO_2 and high reduction ability of g-C_3N_4. However, it was concluded that photoabsorption of sulfur-doped TiO_2 and small specific surface area of g-C_3N_4 are bottlenecks for further enhancement of photocatalytic activity.

Tungsten(VI) oxide (WO_3) may be ideal for a combination pair with g-C_3N_4 in the *Z*-scheme reaction because it is well known as an oxidation part photocatalyst for *Z*-scheme photocatalytic water splitting [14]. Moreover, it has larger visible-light absorption than that of sulfur-doped TiO_2. WO_3 without a co-catalyst is thought to be inappropriate for organic decomposition due to inferior reductive potential of the CB for one-electron reduction of oxygen (O_2). Therefore, a co-catalyst metal for multi-electron reduction of O_2 [20,21] or a reduction part semiconductor with sufficient negative CB potential for one-electron reduction of O_2 in the *Z*-scheme reaction [15–17] is necessary for complete oxidation of organic compounds over WO_3. Although there have been some reports of composite photocatalysts with g-C_3N_4 including g-C_3N_4/WO_3 [7,9–11,22–24], a charge separation mechanism was employed in those photocatalysts, and explanation of the mechanism was not sufficient. Complete oxidation of organic compounds into carbon dioxide (CO_2) was not discussed in photocatalytic evaluation.

In this study, a composite of g-C_3N_4, which was prepared by heat treatment of melamine [25], and WO_3 was prepared by using a planetary mill and its photocatalytic activity for acetaldehyde decomposition was discussed from the viewpoint of complete oxidation into CO_2. Moreover, g-C_3N_4 with a large specific surface area, which was obtained by hydrothermal treatment of original g-C_3N_4 in sodium hydroxide (NaOH) solution [26], was used for the composite photocatalyst in order to improve photocatalytic activity.

2. Experimental

2.1. Materials

All chemicals were reagent grade and used without further purification. g-C_3N_4 powder was synthesized by heating 30 g of melamine at 823 K at a heating rate of 9 K min^{-1}, followed by heating for 4 h at that temperature. The product was collected and ground into powder. WO_3 powders were commercial samples (Kojundo Chemical Laboratory Co.).

2.2. Hydrothermal treatment of g-C_3N_4 in NaOH solution

The specific surface area of g-C_3N_4 was enlarged by hydrothermal method [26]. One gram of as-prepared g-C_3N_4 powder was added to 50 mL of 0.1 M aqueous NaOH solution. The suspension was ultrasonicated for 10 min to completely disperse the g-C_3N_4, and then it was heated in a Teflon-lined autoclave at 373 K for 24 h. After the treatment, the precipitates were centrifuged and washed with deionized water several times to remove Na^+ ion and then dried in a vacuum drying oven at 333 K overnight. This sample is denoted as HT-g-C_3N_4.

2.3. Preparation of a composite photocatalyst by a planetary mill

The composite sample of WO_3 and original g-C_3N_4 was prepared as follows. One gram of WO_3 and original g-C_3N_4 powder and 20 mL of deionized water were added to a 50 mL agate bowl containing 50 g of yttrium-stabilized zirconia grinding beads (Nikkato Co.,=0.6 mm). Then the agate bowl was put on a planetary mill (Fritsch Japan Co., Planetary Micro Mill pulverisette 7) and the planetary mill was operated at 750 rpm for 10 min. After removing the beads by screening, the sample was separated by filtration, washed with deionized water several times, and dried in a vacuum drying oven at 333 K overnight. This composite sample is denoted as CNW*x*, where *x* is the weight percent of WO_3 included in the composite sample. The composite sample of WO_3 and HT-g-C_3N_4 was prepared by the same procedure as that for CNW*x*. This composite sample is denoted as HTW*x*. As a reference, each sample, i.e., original g-C_3N_4, HT-g-C_3N_4 and WO_3, was treated by the same procedure. These composite samples are denoted as CNW0, HTW0 and PM-WO_3, respectively.

2.4. Characterization

Crystal structures of the obtained samples were characterized by an X-ray diffractometer (Rigaku, MiniFlex II) equipped with a Cu *K*α irradiation source. The morphology of prepared particles was observed by field emission scanning electron microscopy (FE-SEM; JEOL, JSM-6701FONO). Diffuse reflectance spectra (DRS) were measured using a UV–vis spectrophotometer (Shimadzu, UV-2600) equipped with an integrating sphere unit (Shimadzu, ISR-2600 Plus). Specific surface area (S_{BET}) was determined with a surface area analyzer (Quantachrome, Nova 4200e) by the Brunauer–Emmett–Teller method. Functional group vibrations were confirmed by using a Fourier transform infrared spectrometer (FTIR; JASCO, FT/IR 4200) with a diffuse reflectance accessory (JASCO, DR-81). Fluorescence spectra were obtained using a photoluminescence spectrometer (JASCO, FP-8500).

2.5. Photocatalytic measurement

Before evaluation of the photocatalytic activity, each sample was irradiated with UV light using black light (UVP, XX-15BLB) in order to remove organic contaminants on the sample. The photocatalytic activity of the composite sample was evaluated by CO_2 liberation from photocatalytic mineralization of acetaldehyde. One hundred milligrams of powder, which has complete extinction of incident radiation, was spread on the bottom of a glass dish, and the glass dish was placed in a Tedlar bag (AS ONE Co. Ltd.). Then 125 cm^3 artificial air containing 1000 ppm of acetaldehyde was injected into the bag. Photoirradiation was performed at room temperature after the acetaldehyde had reached adsorption equilibrium. A light-emitting diode (LED; Epitex, L435-30M32L), which emitted light at wavelengths of ca. 435 nm, was used as a light source, and its intensity was controlled by 1.0 mW cm^{-2}. The concentration of CO_2 was observed by gas chromatography (Shimadzu GC-8A, FID detector) equipped with a Porapak N packed column and a methanizer (GL Science, MT-221) as a function of irradiation time.

3. Results and discussion

3.1. Characterization of g-C_3N_4 and HT-g-C_3N_4

Fig. 1A shows X-ray diffraction (XRD) patterns of original g-C_3N_4 and HT-g-C_3N_4 samples. The original g-C_3N_4 had two peaks at 13.1° and 27.6°, which can be indexed as (1 0 0) and (0 0 2) diffraction planes (JCPDS 87-1526). Similarly, the XRD pattern of HT-g-C_3N_4 also had characteristic peaks at 27.6°, suggesting that HT-g-C_3N_4 has the same crystal structure as that of original g-C_3N_4 (Fig. 1C). The low-angle reflection peak at 13.1° becomes less pronounced due to decreased planar size of the layers during NaOH solution etching of original g-C_3N_4 [26,27]. Functional groups of original g-C_3N_4 and HT-g-C_3N_4 were confirmed by FT-IR spectroscopy. As shown in Fig. 1B, the characteristic IR spectrum of HT-g-C_3N_4 was similar to that of original g-C_3N_4: a peak at about 810 cm^{-1} originating from the heptazine ring system and peaks in the region from 900 to 1800 cm^{-1} attributed to either trigonal C–N(–C)–C or bridging C–NH–C units were observed in both samples. UV–vis DRS are shown in Fig. 1C. Compared with the spectrum of original g-C_3N_4, the spectrum of HT-g-C_3N_4 was shifted to longer wavelengths. A

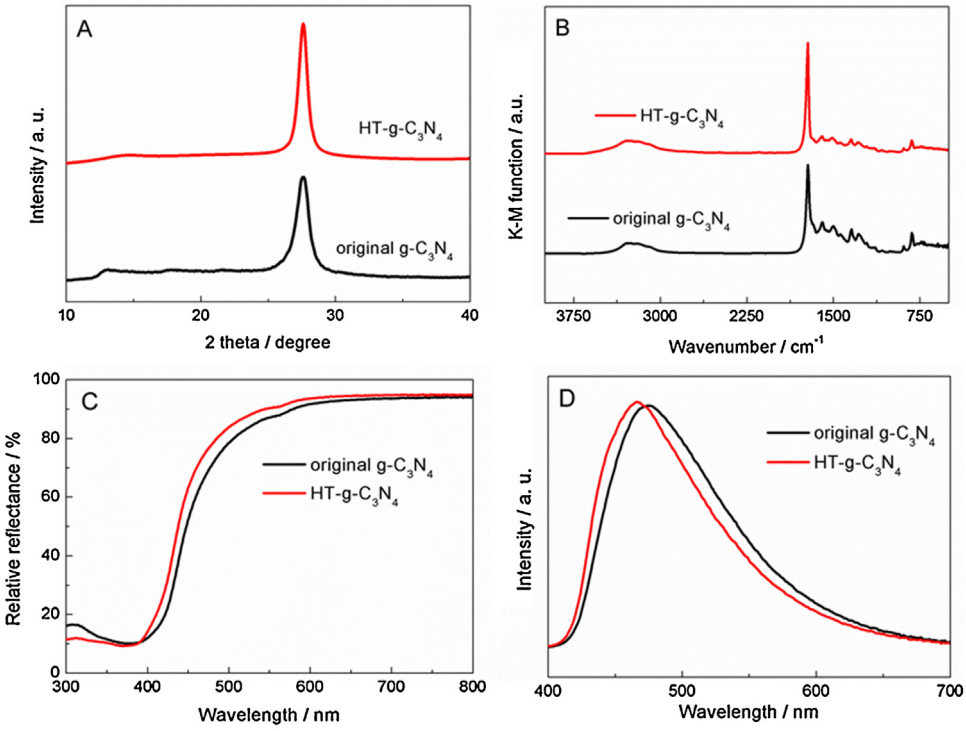

Fig. 1. (A) XRD patterns, (B) FTIR spectra, (C) UV–vis DRS and (D) fluorescence emission spectra under excitation at the wavelength of 365 nm of original g-C_3N_4 and HT-g-C_3N_4.

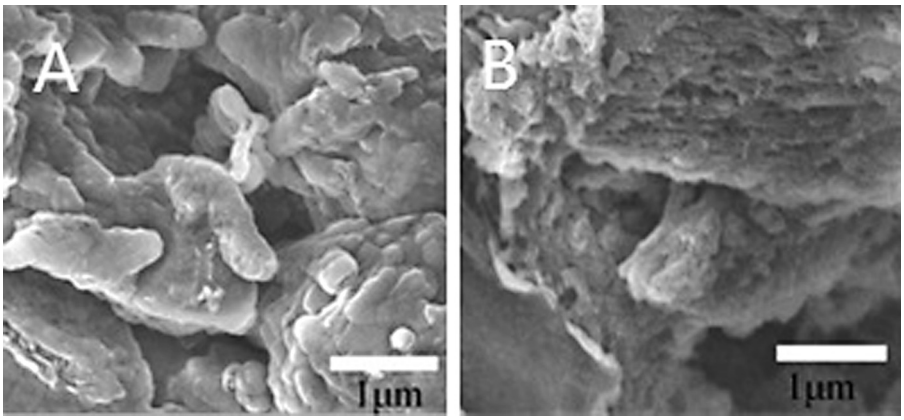

Fig. 2. SEM images of (A) original g-C_3N_4 and (B) HT-g-C_3N_4.

similar blue shift of peak wavelength was observed in fluorescence emission spectra (Fig. 1D). These results are presumably due to decrease in particle size [27,28]. Actually, the S_{BET} of g-C_3N_4 was enlarged from 11 to 50 m^{-2} g^{-1} by hydrothermal treatment. Fig. 2 shows SEM images of original g-C_3N_4 and HT-g-C_3N_4 samples. The original g-C_3N_4 was plate-like particles (Fig. 2A), while HT-g-C_3N_4 had an uneven surface (Fig. 2B). This indicates that the surface of g-C_3N_4 particles was etched by hydrothermal treatment in NaOH solution, resulting in enlargement of S_{BET} without any change in crystal structure. These results coincide with the results of reported study [26].

Photocatalytic activity of original g-C_3N_4 and HT-g-C_3N_4 was evaluated by CO_2 liberation from decomposition of acetaldehyde. Fig. 3 shows the time courses of CO_2 liberation over original g-C_3N_4 and HT-g-C_3N_4. Although HT-g-C_3N_4 showed smaller visible-light absorption than that of original g-C_3N_4, it showed 3-times greater CO_2 liberation due to large S_{BET}, which increase in adsorption, reduction and oxidation sites. However, CO_2 liberation for 48 h was

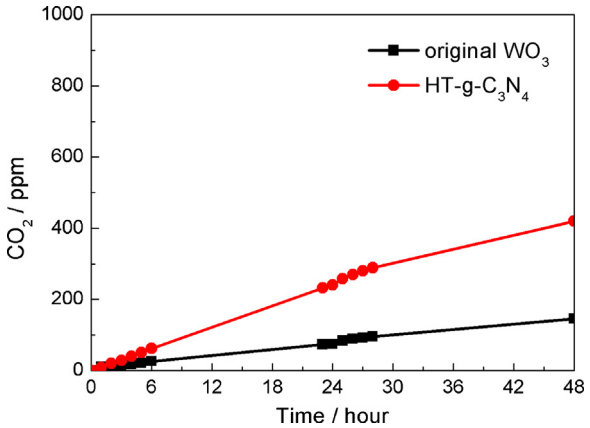

Fig. 3. Time courses of CO_2 liberation from acetaldehyde decomposition over original g-C_3N_4 and HT-g-C_3N_4.

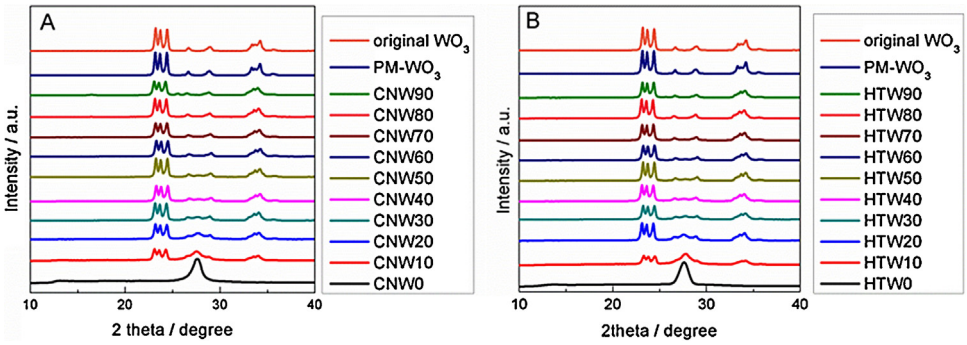

Fig. 4. XRD patterns of original WO_3, PM-WO_3, CNW*x* and HTW*x* samples.

much smaller than 2000 ppm, which means complete decomposition of acetaldehyde into CO_2, due its low oxidation ability [19].

3.2. Characterization of CNWx and HTWx

Powder XRD patterns of CNW*x* samples are shown in Fig. 4A. XRD patterns showed only peaks attributed to g-C_3N_4 and WO_3, and peaks attributed to other components were not detected. Although a peak at 27.6°, which was attributed to (002) of g-C_3N_4, was observed in XRD patterns of CNW*x* ($x < 50$) samples, XRD patterns of CNW*x* ($x > 50$) samples showed no appreciable peak around 27.6° due to weak diffraction intensity of g-C_3N_4. On the other hand, peaks attributed to WO_3 could be observed in all CNW*x* samples ($x > 0$), and no changes in peak pattern and width of the peak at 24.3° were observed, compared with original WO_3 (Fig. 4, S1). This is reasonable since PM-WO_3 showed the same pattern and width of peak at 24.3° as original WO_3. In contrast, CNW0 showed a larger peak width at 27.6° than that of original g-C_3N_4. This result coincides with enlargement of S_{BET} by planetary mill treatment (Fig. 5). A similar result was obtained for HTW*x* samples (Fig. 4B).

Fig. 6 shows SEM images of PM-WO_3, CNW*x* and HTW*x*. PM-WO_3 showed aggregated particles with particle size of a few hundreds of nanometers (Fig. 5), and the morphology and S_{BET} of WO_3 particles were slightly changed by planetary mill treatment (Fig. 5). On the other hand, plate-like particles were pulverized into small particles by the planetary mill treatment in SEM images of CNW0 and HTW0 samples (Fig. S2). This agreed with increase in S_{BET} (Fig. 5). For CNW*x* ($x > 0$) samples, it seemed that WO_3 particles attached to the surface of g-C_3N_4 increased with an increase

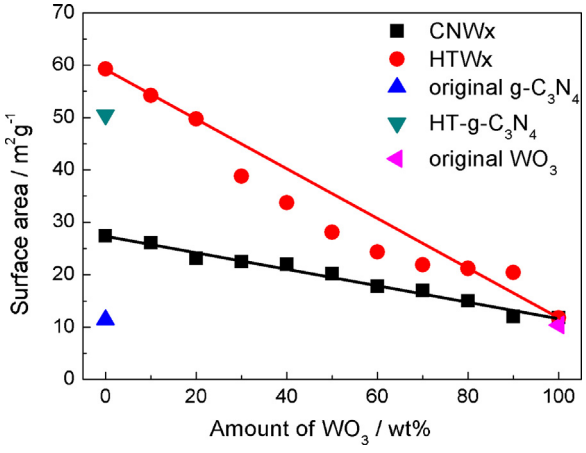

Fig. 5. S_{BET} of original g-C_3N_4, HT-g-C_3N_4, original WO_3, PM-WO_3, CNW*x* and HTW*x* samples as a function of WO_3 content.

in WO_3 content. When the WO_3 content was above 80 wt%, the g-C_3N_4 particles were almost completely covered by WO_3 particles. The same result was also found in HTW*x* ($x > 0$) samples.

Fig. 7 shows UV–vis DRS of PM-WO_3, CNW*x* and HTW*x*. DRS of CNW0 and HTW0 were blue-shifted compared with those of original g-C_3N_4 and HT-g-C_3N_4 (Fig. S3). This blue shift is presumably due to decrease in particle size by planetary mill treatment [27,28], as observed in S_{BET}. Photoabsorption at the wavelength of 435 nm of HTW*x* samples increased with increase in WO_3 content, and it was smaller than CNW*x* (Fig. 8A). This is because PM-WO_3 has the

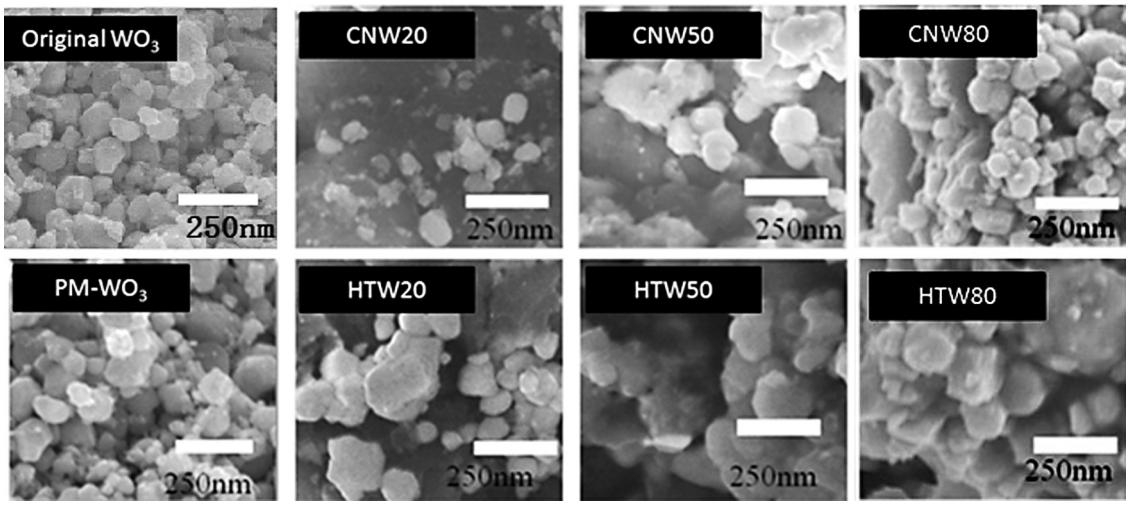

Fig. 6. SEM images of original WO_3, PM-WO_3, CNW*x* and HTW*x* samples with 250 nm size bar.

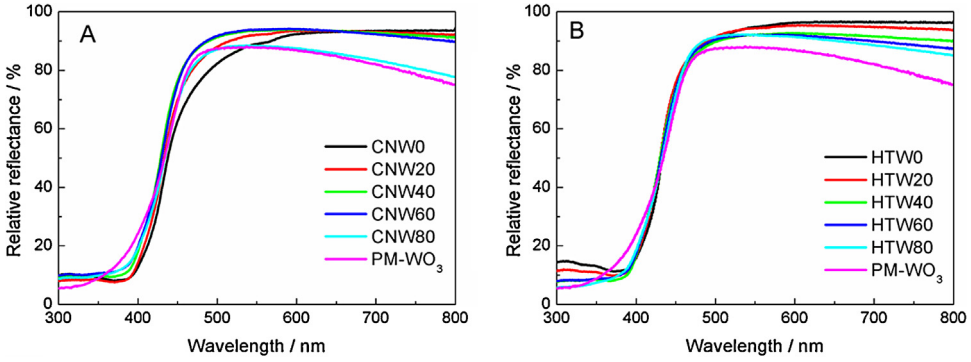

Fig. 7. UV–vis DRS of (A) CNW*x*, (B) HTW*x* and PM-WO_3 samples.

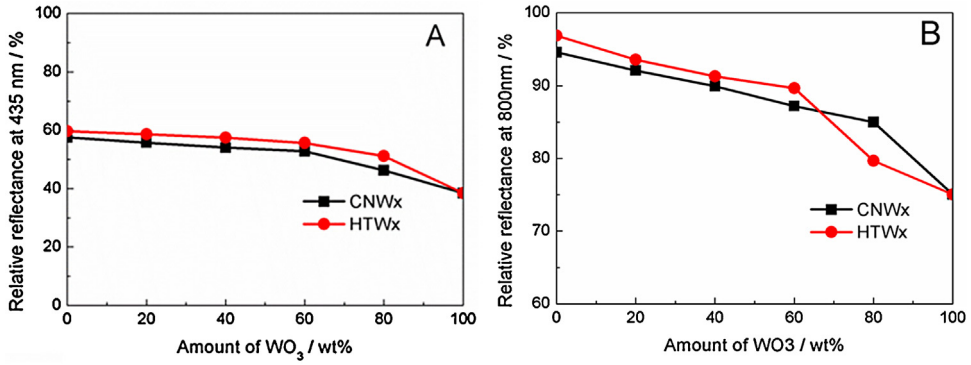

Fig. 8. Relative reflectance of CNW*x* and HTW*x* samples at the wavelengths of (A) 435 nm and (B) 800 nm as a function of WO_3 content.

largest photoabsorption at the wavelength of 435 nm, followed in order by CNW0 and HTW0. On the other hand, photoabsorption at a longer wavelength of 500 nm, which was observed in the DRS of WO_3, was suppressed by composition with a small amount of g-C_3N_4. Fig. 8B shows relative reflectance of CNW*x* and HTW*x* samples at the wavelength of 800 nm as a function of WO_3 content. CNW*x* and HTW*x* samples showed no linear relationship between relative reflectance at the wavelength of 800 nm and WO_3 content. Since photoabsorption at a longer wavelength of 500 nm is attributed to the W^{5+} state in WO_3, which is generated by electron accumulation

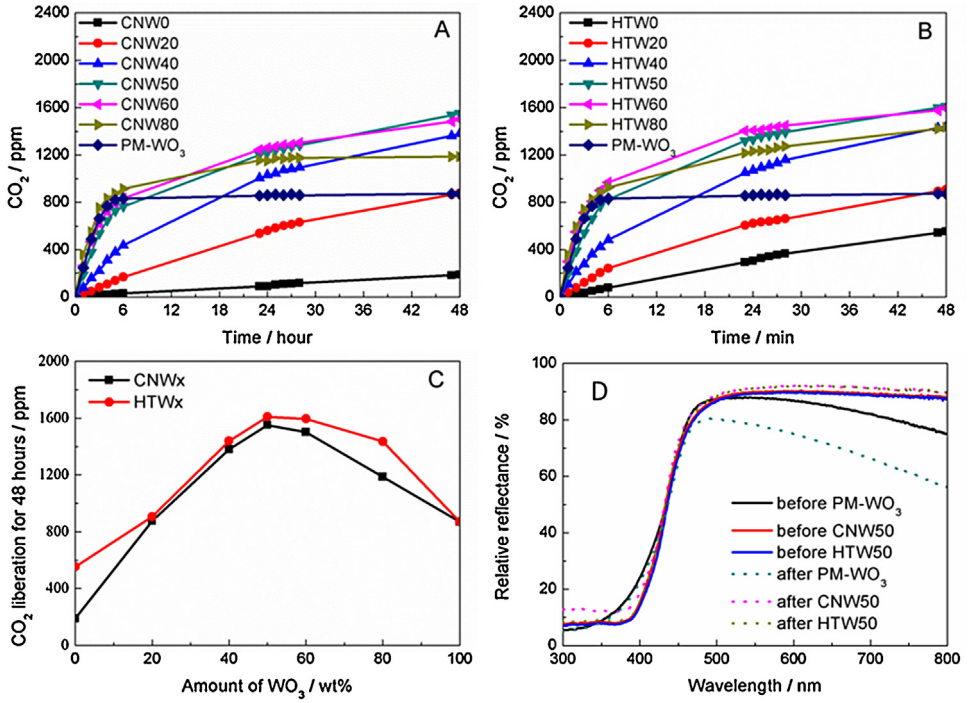

Fig. 9. Time courses of CO_2 liberation from acetaldehyde decomposition over (A) CNW*x* and (B) HTW*x* samples. (C) CO_2 liberation over CNW*x* and HTW*x* samples for 48 h of photoirradiation as a function of WO_3 content. (D) UV–vis DRS of PM-WO3, CNW50 and HTW50 before and after photocatalytic reaction.

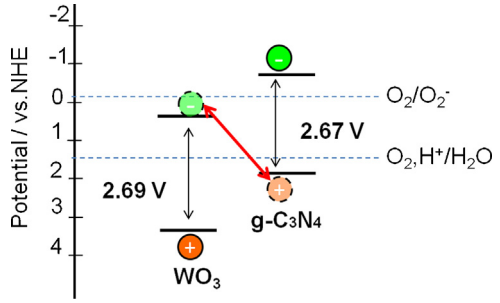

Fig. 10. Schematic band structure of g-C_3N_4 and WO_3. The literature values for the band structure of g-C_3N_4 [32] and WO_3 [33] were used.

in WO_3 and reduction treatment of WO_3 [29–31], a nonlinear relationship means that electron accumulation in WO_3 was decreased by composition with g-C_3N_4. A similar phenomenon was observed in the *Z*-scheme composite photocatalyst of WO_3 and $CaFe_2O_4$ [13].

3.3. Photocatalytic activity for acetaldehyde decomposition

The photocatalytic activities of the prepared samples were evaluated by CO_2 liberation from photocatalytic mineralization of acetaldehyde. Fig. 9A shows the time courses of CO_2 liberation of the CNW*x* samples and PM-WO_3. WO_3 showed a high CO_2 liberation rate at the beginning of photoirradiation, but CO_2 liberation stopped with longer photoirradiation before reaching 2000 ppm, which means complete decomposition of 1000 ppm acetaldehyde. WO_3 can partially decompose acetaldehyde to formaldehyde or formic acid with CO_2 liberation [15], but it cannot completely decompose these molecules to CO_2 without efficient electron consumption [16]. In contrast, almost all of the composite samples showed no saturation tendency of CO_2 liberation with irradiation time and a larger amount of CO_2 liberation for 48 h. This implies that electron consumption in WO_3 was promoted by composition with g-C_3N_4, as observed in WO_3 composed with other semiconductors or metals [15–17,20,21]. Actually, results from UV–vis DRS of CNW*x* and HTW*x* samples indicate that electron accumulation in WO_3 is suppressed by composition of g-C_3N_4 (Fig. 8B). Since g-C_3N_4 is a semiconductor with more negative CB potential than that of WO_3 and one-electron reduction potential of O_2, a plausible mechanism is *Z*-scheme reaction accompanied by electron transfer from the CB of WO_3 to the VB of g-C_3N_4 (Fig. 10). Thus, all WO_3 particles are required to be attached on all g-C_3N_4 particles for efficient charge transfer. Otherwise, acetaldehyde on non-composite g-C_3N_4 and WO_3 remained without being decomposed completely into CO_2. This is the reason why CNW*x* with a large amount of WO_3 showed a saturation tendency and CNW*x* with a small amount of WO_3 showed a low rate of CO_2 liberation.

Fig. 9B shows the time courses of CO_2 liberation of the HTW*x* composites and PM-WO_3. HTW*x* samples also showed similar enhancement for CO_2 liberation by the composition as observed in CNW*x* samples. However, HTW*x* ($x > 0$) samples showed slightly larger CO_2 liberation than that of CNW*x* ($x > 0$), though CO_2 liberation of HTW0 was twice larger than that of CNW0 for 48 h. This can be explained as follows. g-C_3N_4 in composite samples predominantly works as not an adsorption and oxidation site for organic compounds but a reduction site for O_2, while adsorption, oxidation and reduction must all proceed on single g-C_3N_4. Therefore, enhancement of S_{BET} of g-C_3N_4 in a composite sample is thought to show no direct contribution to oxidation of acetaldehyde because acetaldehyde is hardly decomposed over g-C_3N_4 in the composite photocatalyst.

Fig. 9C shows CO_2 liberation for 48 h of CNW*x* and HTW*x* samples as a function of WO_3 content. A volcano-like relationship was observed in both CNW*x* and HTW*x* samples, but HTW*x* samples with a larger amount of WO_3 showed larger CO_2 liberation because larger S_{BET} of g-C_3N_4 in HTW*x* samples increased contact points between g-C_3N_4 and WO_3. However, optimized HTW*x* showed slightly larger CO_2 liberation than that of CNW*x*, and the optimum ratio of WO_3 in HTW*x* samples was the same as that in CNW*x* samples despite larger S_{BET}. This is due to smaller photoabsorption of HTW0 than that of CNW0, as seen in Fig. 8A.

Fig. 9D shows UV–vis DRS of PM-WO_3, CNW50 and HTW50 before and after photocatalytic reaction. After photocatalytic reaction, photoabsorption of PM-WO_3 at wavelengths from 500 nm to 800 nm showed greatly increased, which is attributed to the partial reduction of W^{6+} to W^{5+} by photoexcited electrons. In the case of CNW50 and HTW50, no obvious changes can be found from DRS of the composite photocatalysts before and after photocatalytic reaction. The results indicate that the self-reduction process by photogenerated electrons in WO_3 are prevented after composite with g-C_3N_4 or HT-g-C_3N_4, because photogenerated electrons in CB of WO_3 should be efficiently consumed by the reaction with photogenerated holes in VB of g-C_3N_4 or HT-g-C_3N_4. This means that the composite photocatalysts follow *Z*-scheme charge separation mechanism.

Larger CO_2 liberation over composite samples may be attributed to decomposition of g-C_3N_4. Therefore, we confirmed stability of g-C_3N_4 in the prepared samples by a self-decomposition test. Fig. S4 shows the time courses of CO_2 liberation over CNW50 and HTW50 in the presence and absence of acetaldehyde. Although slight CO_2 liberation was observed in CNW50 and HTW50 samples, it was much smaller than CO_2 liberation in the presence of acetaldehyde. This confirmed that enlargement of CO_2 was not due to decomposition of g-C_3N_4. In the HTW50 sample, 1600 ppm of CO_2 was observed after 48 h of photoirradiation, indicating that at least 600 ppm of acetaldehyde had been completely decomposed into 1200 ppm of CO_2. This "partial complete oxidation" is also collateral evidence for *Z*-scheme charge transfer in the composite photocatalyst because complete oxidation of acetaldehyde into CO_2 cannot occur over WO_3 without a metal co-catalyst or semiconductor for *Z*-scheme charge transfer.

4. Conclusions

In this study, a highly active photocatalyst under visible-light irradiation for organic decomposition was synthesized by a composite of g-C_3N_4 and WO_3 using a planetary mill. UV–vis DRS and photocatalytic evaluation indicated that the composite photocatalysts show high activity as a result of *Z*-scheme reaction. The optimized composite samples prepared in the present study showed complete oxidation of "most of all" acetaldehyde into CO_2 by *Z*-scheme reaction, unlike previously reported composite photocatalysts [22–24]. For further enhancement of photocatalytic activity under visible-light irradiation, a composite photocatalyst with both large visible-light absorption and a large number of contact points between g-C_3N_4 and WO_3 is needed.

Acknowledgments

This work was supported by the JST PRESTO program and the JST ACT-C program.

Appendix A. Supplementary data

Supplementary material related to this article can be found, in the online version, at http://dx.doi.org/10.1016/j.apcatb.2013.12.048.

References

[1] K. Hashimoto, H. Irie, A. Fujishima, Japanese Journal of Applied Physics 44 (2005) 8269–8285.
[2] T. Ohno, M. Akiyoshi, T. Umebayashi, K. Asai, T. Mitsui, M. Matsumura, Applied Catalysis A: General 265 (2004) 115–121.
[3] T. Ohno, T. Tsubota, K. Nishijima, Z. Miyamoto, Chemistry Letters 33 (2004) 750–751.
[4] S. Sato, J.M. White, Journal of the American Chemical Society 102 (1980) 7206–7210.
[5] N. Murakami, Y. Kurihara, T. Tsubota, T. Ohno, Journal of Physical Chemistry C 113 (2009) 3062–3069.
[6] T. Ohno, K. Sarukawa, M. Matsumura, New Journal of Chemistry 26 (2002) 1167–1170.
[7] S.C. Yan, S.B. Lv, Z.S. Li, Z.G. Zou, Dalton Transactions 39 (2010) 1488–1491.
[8] A.K. Chakraborty, M.A. Kebede, Reaction Kinetics, Mechanisms and Catalysis 106 (2012) 83–98.
[9] Q. Xiang, J. Yu, M. Jaroniec, Journal of Physical Chemistry C 115 (2011) 7355–7363.
[10] G.Z. Liao, S. Chen, X. Quan, H.T. Yu, H.M. Zhao, Journal of Materials Chemistry 22 (2012) 2721–2726.
[11] C. Pan, J. Xu, Y. Wang, D. Li, Y. Zhu, Advanced Functional Materials 22 (2012) 1518–1524.
[12] N. Serpone, P. Maruthamuthu, P. Pichat, E. Pelizzetti, H. Hidaka, Journal of Photochemistry and Photobiology A: Chemistry 85 (1995) 247–255.
[13] Z.F. Liu, Z.G. Zhao, M. Miyauchi, Journal of Physical Chemistry C 113 (2009) 17132–17137.
[14] R. Abe, Bulletin of the Chemical Society of Japan 84 (2011) 1000–1030.
[15] T. Arai, M. Horiguchi, M. Yanagida, T. Gunji, H. Sugihara, K. Sayama, Journal of Physical Chemistry C 113 (2009) 6602–6609.
[16] T. Arai, M. Yanagida, Y. Konishi, Y. Iwasaki, H. Sugihara, K. Sayama, Catalysis Communications 9 (2008) 1254–1258.
[17] T. Arai, M. Yanagida, Y. Konishi, Y. Iwasaki, H. Sugihara, K. Sayama, Journal of Physical Chemistry C 111 (2007) 7574–7577.
[18] X.C. Wang, K. Maeda, A. Thomas, K. Takanabe, G. Xin, J.M. Carlsson, K. Domen, M. Antonietti, Nature Materials 8 (2009) 76–80.
[19] K. Kondo, N. Murakami, C. Ye, T. Tsubota, T. Ohno, Applied Catalysis B: Environmental 142–143 (2013) 362–367.
[20] R. Abe, H. Takami, N. Murakami, B. Ohtani, Journal of the American Chemical Society 130 (2008) 7780–7781.
[21] T. Arai, M. Horiguchi, M. Yanagida, T. Gunji, H. Sugihara, K. Sayama, Chemical Communications (2008) 5565–5567.
[22] K. Katsumata, R. Motoyoshi, N. Matsushita, K. Okada, Journal of Hazardous Materials 260 (2013) 475–482.
[23] H. Yan, X. Zhang, S. Zhou, X. Xie, Y. Luo, Y. Yu, Journal of Alloys and Compounds 509 (2011) L232–L235.
[24] L. Huang, H. Xu, Y. Li, H. Li, X. Cheng, J. Xia, Y. Xua, Guobin Caia, Dalton Transactions 42 (2013) 8606–8616.
[25] S.C. Yan, Z.S. Li, Z.G. Zou, Langmuir 25 (2009) 10397–10401.
[26] T. Sano, S. Tsutsui, K. Koike, T. Hirakawa, Y. Teramoto, N. Negishi, K. Takeuchi, Journal of Materials Chemistry A 1 (2013) 6489–6496.
[27] M. Groenewolt, M. Antonietti, Advanced Materials 17 (2005) 1789–1792.
[28] P. Niu, L.L. Zhang, G. Liu, H.M. Cheng, Advanced Functional Materials 22 (2012) 4763–4770.
[29] M. Fujii, T. Kawai, H. Nakamatsu, S. Kawai, Journal of the Chemical Society, Chemical Communications (1983) 1428–1429.
[30] Y. He, Z. Wu, L. Fu, C. Li, Y. Miao, L. Cao, H. Fan, B. Zou, Chemistry of Materials 15 (2003) 4039–4045.
[31] M. Miyauchi, M. Shibuya, Z. Zhao, Z. Liu, Journal of Physical Chemistry C 113 (2009) 10642–10646.
[32] J.S. Zhang, X.F. Chen, K. Takanabe, K. Maeda, K. Domen, J.D. Epping, X.Z. Fu, M. Antonietti, X.C. Wang, Angewandte Chemie International Edition 49 (2010) 441–444.
[33] Y. Xu, M.A.A. Schoonen, American Mineralogist 85 (2000) 543–556.